CSCE Annual Conference

Growing with youth – Croître avec les jeunes

Laval (Greater Montreal)

June 12 - 15, 2019

NUMERICAL INVESTIGATION OF CONCRETE-FILLED STEEL SQUARE COLUMNS SUBJECTED TO CONCENTRIC AND ECCENTRIC LOADING

Rahman, S.[1], Islam, K.[2,4], Ibrahim, I.[1] and Ahmed, A.[3]
[1]Military Institute of Science and Technology, Bangladesh
[2]Polytechnique Montreal, Canada
[3]University of Wollongong, Australia
[4]kamrul.islam@polymtl.ca

Abstract: This paper presents a numerical study on the compressive behaviour of concrete-filled steel square columns subjected to concentric and eccentric loading conditions. Numerical models are developed using general purpose finite element (FE) software ABAQUS and have been validated using the available test results in the literature. The FE models predict the experimental load-deformation curve, ultimate strength and failure modes with good accuracy. Furthermore, the experimentally validated FE models are used to carry out a series of parametric study to investigate the effect of geometric and material properties on the behaviour of concentrically and eccentrically loaded concrete-filled steel square columns. Concrete compressive strength, steel yield strength, column depth to thickness ratio, and load eccentricity ratio are the key parameters that are varied in the FE models to assess their effect on the ultimate behaviour of concrete-filled steel columns. Finally, numerical results are compared with the existing AISC design guideline which clearly shows conservative nature of code predictions.

1 Introduction

Concrete-filled steel tubular (CFST) columns are a widely used composite column exhibiting excellent composite action between steel tubes and core concrete. Steel tubes provide confinement of the core concrete, thereby increasing significantly its strength and ductility. On the other hand, core concrete delays the inward buckling of the steel tube. As a further benefit of this novel method, no form-works are needed during construction, which significantly reduces the construction time and cost. CFST columns generally exhibit higher strength, stiffness, ductility, energy dissipation, and better seismic resistance compared to reinforced concrete or steel columns. Therefore, the popularity of CFST columns is increasing all over the world for the construction of bridges and mid-rise to high-rise buildings. For example, CFST columns were used in the recent construction of the well-known Taipei 101 skyscraper (Shieh et al. 2003).

In recent decades, extensive experimental studies have been carried out on the behaviour of CFST columns under pure compression, compression plus bending, and pure torsion (Han 2002, Shams and Saadeghvaziri 1997, Schnieder 1998, Han et al. 2007, Han et al. 2005, Yu et al. 2010, Sakino et al.1985, Huang et al. 2012, Liu et al. 2008, Zhang et al. 2009, Perea et al. 2014, Jiang et al.2013, Yang and Ma 2013). The results of these studies indicate that the overall behaviour of CFST columns depends on the strength of steel and core concrete, the geometric shape of the steel section, the thickness of the steel tubes, the column slenderness ratio, the given steel tube fabrication process used (hot-rolled versus built-up) and the loading condition (eccentric versus concentric). Currently available design standards, such as

the American Institute of Steel Construction (AISC), Eurocode 4 (EC4), Canadian Standard Association (CSA S16-09), and Australian Steel Standard (AS 5100) impose restrictions on the use of high strength steel (HSS) and high strength concrete (HSC) in CFST columns. In this context, limited experimental research has been carried out on CFST columns utilizing HSS and HSC (Liu and Gho 2005, Thai et al. 2014, Khan et al. 2016, Khan et al. 2017). However, experimental studies on the behaviour of large (a cross-section greater than 450 mm) CFST columns are still rare (Chen et al. 2012). There is thus a need for an investigation of the behaviour of CFST columns having a large cross-section (greater than 450 mm) deployed in high-rise buildings.

Numerical modelling is gaining popularity in the field of composite structures. This method uses commercially available finite element (FE) analysis software, given the accuracy of FE modelling to predict the behaviour of structural elements under different loading conditions. It is also worth noting that experimental studies, as an alternative method, are highly expensive, time-consuming, and difficult to conduct. Numerical simulations of CFST columns, meanwhile, have been performed by Ellobody and Young 2006, Han et al. 2007, Tao et al. 2013, Thai et al. 2014, and Khan et al. 2017. However, the results of the FE models developed in these studies are highly dependent on the material modelling, local and global imperfection magnitude, steel-concrete interaction property, residual stress pattern, and support condition. Different authors have adopted different techniques to model the behaviour of CFST columns, and this affects the magnitude of the ultimate strength of the CFST columns. Therefore, it is important to adopt a consistent methodology to simulate the behaviour of CFST columns which is well aligned with the experimental results. In this regard, a combined experimental and numerical study along with a series of parametric studies is capable of expanding the existing experimental results over a wider range of concrete and steel strengths, column depth-to-thickness ratios, and load eccentricity ratios.

The objectives of the study presented in this paper are three-fold: the first is to develop a refined FE model of CFST columns and to verify the developed FE models through available test results from past literature, the second is to perform a comprehensive parametric study to identify the parameters that influence the behaviour of CFST columns, and the third is to compare the numerical results with the current AISC design standard.

2 Numerical Modelling

2.1 Development of the Finite Element Model

In this study, 4-node shell elements with reduced integration and hourglass control (S4R) and 8-node brick element with reduced integration and three translational degrees of freedom at each node (C3D8R), were used to model steel tube and core concrete. The assigned mesh size in the FE models was equal to B/15 across the cross section with an element aspect ratio of 3 along the length of the specimen. This mesh size was selected based on previous numerical studies of CFST columns (Tao et al. 2013 and Khan et al. 2017). Figure 2(a) shows the 3D meshed FE model of a typical CFST column.

2.2 Boundary Condition and Initial Imperfection Modelling

In this study, concentrically loaded CFST columns were modelled considering fixed-ended boundary condition, where longitudinal displacement was allowed at the top end of the column. Each of the nodes of the top and bottom ends of columns were coupled with two reference points located at the centre of the column specimen. All 6 degrees of freedom of the bottom and top reference points were restrained except the longitudinal translation of the top reference point (loaded end). The boundary condition for concentrically loaded column is shown in Figure 2(a). Eccentrically loaded CFST columns were modelled considering pin-ended boundary condition, where each of the nodes of the top and bottom ends were tied with two eccentric reference points (i.e., ‘e’ mm from the centre of the cross-section) through rigid body constraints. All translational and rotational degrees of freedom, with the exception of rotation around the *x*-axis for the bottom end, were restrained. In the case of the top (loaded) end, all translational and rotational degrees of freedom, with the exception of longitudinal translation and rotation around the *x*-axis, were restrained to satisfy the pin-ended boundary condition. The load was applied to the top reference point in both concentric and eccentric columns using the displacement control technique.

Initial imperfection has a significant effect on the behaviour of CFST columns (Tao et al. 2013 and Khan et al. 2017). In this study, initial imperfection was accounted for in the numerical modelling technique using the *IMPERFECTION option available in ABAQUS. To quantify the shape of the initial geometric imperfection, elastic eigen value buckling analysis was performed, with the first mode shape adopted as the distribution of the initial geometric imperfection. The amplitude of the initial geometric imperfection was set as L/1,000 where L is the length of the column specimen. Residual stress, it should be noted, was not considered in this study, as it has a negligible effect on the behaviour of CFST columns (Thai et al. 2014).

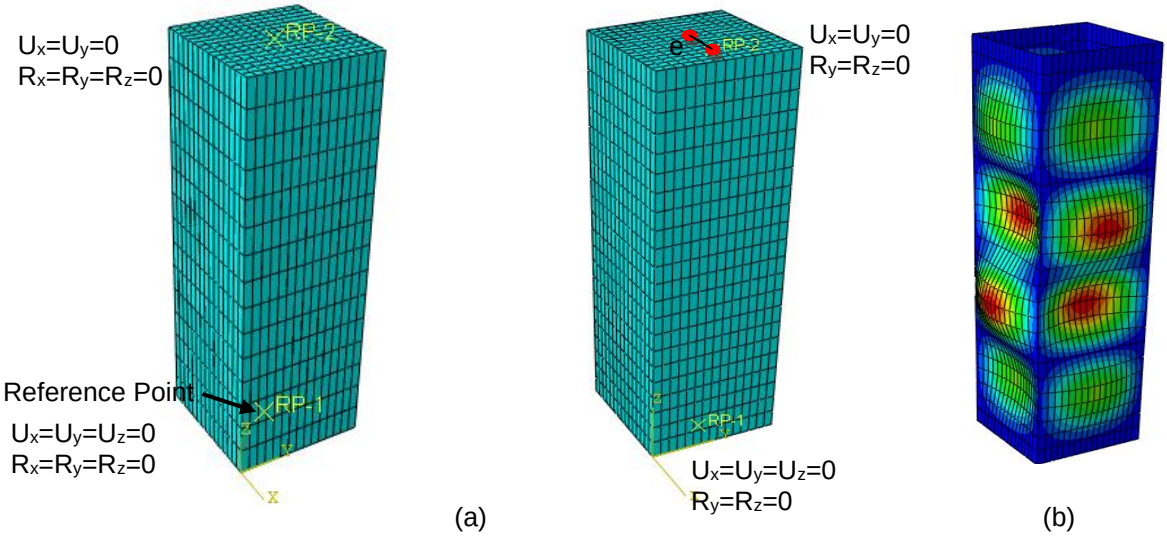

Figure 2: (a) 3D meshed FE model of a typical concentrically loaded and eccentrically loaded CFST column, and (b) first elastic bucking mode shape

2.3 Steel-Concrete Interaction Modelling

The steel-concrete interface was modelled using the surface-to-surface contact option available in ABAQUS. The steel plate surface was defined as the master surface, whereas outer surface of the core concrete was defined as the slave surface. Normal behaviour in the contact modelling was defined using the 'hard contact' algorithm, which allows separation of master and slave surfaces after contact. The tangential behaviour was simulated using the 'Coulomb friction model' with a coefficient of friction value of 0.6 (Tao et al. 2013).

2.4 Material Modelling

Several material modelling techniques are available in the literature to model the behaviour of steel. Among them, the elastic-perfectly plastic model (Tao et al. 2013), elastic-plastic model with liner strain hardening (Guo at al. 2007), and multi-liner hardening model (Han at al. 2017) were used to simulate the behaviour of CFST columns. However, Tao et al. (2013) shows that the three material models yield similar load-axial strain responses of CFST columns. Moreover, square CFST columns show less strain-hardening response compared to circular CFST columns (Tao et al. 2013). Hence, the elastic-perfectly plastic material model forsteel is deemed sufficient to capture the behaviour of square CFST columns. The concrete forthe CFST columns was modelled using the concrete damage plasticity model available in ABAQUS to simulate the nonlinear behaviour of the core concrete material. The key parameters of the damage plasticity models, it should be noted, are modulus of elasticity of concrete (*Ec*), tensile strength of concrete, dilation angle (Ψ), ratio of the second stress invariant on the tensile meridian to that on the compressive meridian (K_c), ratio of the biaxial concrete strength to uniaxial concrete strength (f_{b0}/f'_c), flow potential eccentricity (*e*), and fracture energy (G_F). A detailed description of the confined concrete material modelling technique of CFST columns can be found in Tao et al. (2013).

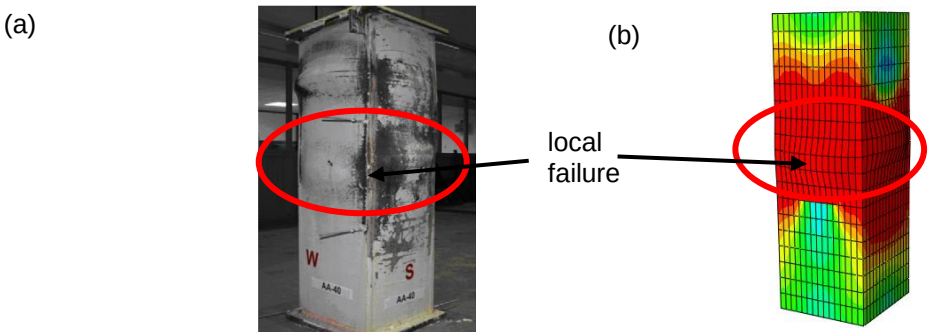

Figure 3: Comparison of deformed shape of the specimen (AA40) obtained from (a) experimental study (Chen et al, 2012) and (b) current numerical study

3 Validation of Numerical Model

Numerically developed FE models were compared with the current and existing test results to assess the accuracy of the numerical modelling technique. In total 68 experimental results of CFST columns were compared with the FE models. Among them, 6 columns from the present study and 62 columns from existing literature were numerically validated. The geometric and material properties used to validate the FE models are shown in Tables 2 and 3. Ultimate load carrying capacity, full load-end shortening curves, and failure modes obtained from FE models were compared with the experimental test results. The numerically quantified peak loads were found to closely match with the experimental values. The final deformed shape of a previously tested CFST column and an FE model is shown in Figure 3. The experimental load-axial deformation curve of 5 CFST stub columns obtained from existing literature and 6 CFST columns tested in this study were compared with the developed FE models as shown in Figure 4. Although the FE models were found to be capable of predicting the experimental results with good accuracy, the difference maybe attributable to the variation in imperfection amplitude incorporated in the FE models as the exact imperfection magnitude of the test specimens were unknown. Overall, the developed FE models were found to be capable of simulating the experimental test results with good accuracy and can be further used to generate additional results to study the behaviour of CFST columns through a parametric study. The key findings of the comparison of experimental and FE results with code-predicted capacity are shown in Table 4.

Table 2: Comparison of experimental and FE results with code predicted capacity for pure compression

Reference	ID	BxDxt (mm)	L (mm)	f_y (MPa)	f'_c (MPa)	Load capacity (kN)			$\frac{P_{FE}}{P_{EXP}}$	$\frac{P_{FE}}{P_{AISC}}$
						P_{EXP}	P_{FE}	P_{AISC}		
Schneider 1998	S1	127x127x3.2	610	356	30.45	912	1017	960	1.12	1.06
	S2	127 x127x4.3	610	357	26.04	1092	1143	1101	1.05	1.04
	S3	127 x127x4.6	610	322	23.80	1103	1067	1028	0.97	1.04
	S4	127 x127x5.7	610	312	23.80	1220	1199	1163	0.98	1.03
	R1	76x152x3.0	608	430	30.45	800	880	857	1.10	1.03
	R2	76 x152x4.5	608	383	26.04	991	1009	986	1.02	1.02
	R3	102 x152x4.3	608	413	26.04	1135	1241	1204	1.09	1.03
	R4	102 x152x4.6	608	365	23.80	1216	1150	1116	0.95	1.03
Han 2005	SB2-1	100x100x2.0	300	404	42.90	770	719	673	0.93	1.07
	SB3-1	150x150x2.0	450	404	42.90	1300	1362	1072	1.05	1.27
	SB4-1	200x200x2.0	600	404	42.90	1990	2194	1496	1.10	1.47
	SC1-2	60x60x2.0	180	404	*71.54	423	419	385	0.99	1.09
	SC2-2	150x150x2.0	450	404	*71.54	1980	1958	1521	0.99	1.29

Han 2002	RC1-1	100x100x2.9	300	228	50.77	760	716	657	0.94	1.09
	RC2-1	120x120 x2.9	360	228	50.77	992	978	896	0.99	1.09
	RC3-1	110x100 x2.9	330	228	50.77	844	779	712	0.94	1.09
	RC4-1	150x135 x2.9	450	228	50.77	1420	1310	1205	0.92	1.09
	RC5-1	90x70 x2.9	270	228	50.77	554	484	449	0.87	1.08
	RC6-1	100x75 x2.9	300	228	50.77	640	561	518	0.88	1.08
	RC7-1	120x90 x2.9	360	228	50.77	800	766	703	0.96	1.09
	RC8-1	140x105 x2.9	420	228	50.77	1044	992	915	0.95	1.08
	RC9-1	150x115 x2.9	450	228	50.77	1251	1137	1050	0.91	1.08
	RC10-1	160x120x7.6	480	228	50.77	1820	1681	1622	0.92	1.04
	RC11-1	130x85x2.9	390	228	50.77	760	779	720	1.03	1.08
	RC12-1	140x80 x2.9	420	228	50.77	880	786	732	0.89	1.07
Chen 2012	AA-48	500x500x10	1500	350	41.20	16500	16518	15390	1.00	1.07
	AA-40	500x500x12	1500	350	41.20	17900	17773	16630	0.99	1.07
	AA-32	410x410x12	1230	350	41.20	12800	13025	12272	1.02	1.06
	AA-24	410x410x16	1230	350	41.20	15300	14863	14263	0.97	1.04

Table 3: Comparison of experimental and FE results with code predicted capacity for combined compression and bending

Reference	ID	B x D x t (mm)	L (mm)	e (mm)	f_y (MPa)	f'_c (MPa)	Load capacity (kN)			$\frac{P_{FE}}{P_{EXP}}$	$\frac{P_{FE}}{P_{AISC}}$
							P_{EXP}	P_{FE}	P_{AISC}		
Wang 2011	GZ-1	150x150x6	866	25	306	37.72	1398	1235	1245	0.88	0.99
	GZ-2	150x150x6	866	50	306	55.12	1224	1064	1156	0.87	0.92
	GZ-3	150 x150x6	866	75	306	75.14*	936	947	978	1.01	0.97
	GZ-4	150 x150x6	1300	25	306	55.12	1356	1358	1460	1.00	0.93
	GZ-5	150 x150x6	1300	50	306	75.14*	1152	1159	1259	1.01	0.92
	GZ-7	150 x150x6	2165	25	306	75.14*	1234	1333	1664	1.08	0.80
	GZ-9	150 x150x6	2165	75	306	55.12	796	706	889	0.89	0.79
Toshiaki 2004	ER4-A-4-19	149x149x4.4	447	200	262	40.5	267	245	222	0.92	1.10
	ER4-A-4-57	148x148 x4.4	444	45	262	40.5	823	815	815	0.99	1.00
	ER4-C-2-25	215x215 x4.4	645	200	262	25.4	503	507	502	1.01	1.01
	ER4-C-2-56	214x214 x4.4	642	60	262	25.4	1141	1184	1190	1.04	0.99
	ER4-C-4-21	215x215 x4.4	645	200	262	40.5	580	586	547	1.01	1.07
	ER4-C-4-38	215x215 x4.4	645	100	262	40.5	1028	1110	1068	1.08	1.04
	ER4-C-8-33	214x214 x4.4	642	100	262	77.0*	1448	1501	1479	1.04	1.01
	ER4-C-8-46	215x215 x4.4	645	60	262	77.0*	2014	2176	2106	1.08	1.03
	ER4-D-4-27	323x323 x4.4	969	200	262	40.5	1479	1599	1479	1.08	1.08
	ER4-D-4-60	323x323 x4.4	969	60	262	40.5	3306	3491	3471	1.06	1.01
	ER6-A-4-22	144x144x6.4	432	200	618*	40.5	611	580	608	0.95	0.95
	ER6-A-4-61	144x144 x6.4	432	45	618*	40.5	1701	1672	1679	0.98	1.00
	ER6-C-2-58	210x210 x6.4	630	60	618*	25.4	2393	2570	2591	1.07	0.99
	ER6-C-4-18	210x210 x6.4	630	300	618*	40.5	858	898	940	1.05	0.96
	ER6-C-4-44	210x210 x6.4	630	100	618*	40.5	2092	2217	2296	1.06	0.97
	ER6-C-4-57	209x209 x6.4	627	60	618*	40.5	2694	2827	2863	1.05	0.99
	ER6-C-8-24	210x210 x6.4	630	200	618*	77.0*	1486	1509	1560	1.02	0.97
	ER6-C-8-54	210x210 x6.4	630	60	618*	77.0*	3396	3459	3668	1.02	0.94
	ER6-D-4-23	319x319 x6.4	957	300	618*	40.5	1969	2191	2218	1.11	0.99
	ER6-D-4-47	319x319 x6.4	957	100	618*	40.5	4045	4635	4847	1.15	0.96

4 Parametric Study

The FE modelling techniques used to validate the experimental test results were adopted to perform an extensive parametric study to investigate the behaviour of CFST columns under concentric and eccentric

loading conditions. All the columns used in the parametric study had a constant cross-sectional dimension of 500 mm × 500 mm (B mm × D mm), representing a fairly large size composite column for a typical high-rise structure. These columns were designed and analyzed during the parametric study to incorporate the effects of several geometric and material parameters that can significantly affect CFST column behaviour. The variables were the load eccentricity ratio (e/D), depth-to-thickness ratio (D/t), concrete compressive strength (f'_c), and yield strength (f_y) of steel. In total 81 FE models were developed for the purpose of the parametric study. The columns were designated according to the form C1D1E1F1, where 'C' refers to the column concrete compressive strength, and the suffixes 1, 2, and 3 under 'C' represent the concrete strengths of 30 MPa, 40 MPa, and 50 MPa, respectively. Similarly, 'D', 'E' and 'F' represent the D/t, e/D, and f_y, respectively. In the case of 'D', suffixes 1, 2, and 3 represent the D/t ratios 30, 40, and 50, respectively. 'E1', 'E2', and 'E3' represent the e/D ratios of 0, 0.15, and 0.3, respectively. Similarly, 'F1', 'F2', and 'F3' represent the steel yield strengths of 250, 350, and 600 MPa, respectively. The results of the 81 FE simulations with varying geometric and material parameters are shown in Figure 5.

Table 4: Comparisons of experimental and FE results with code predicted capacity

No. of Experiments: 66 No of FE models: 147	$\frac{P_{FE}}{P_{EXP}}$	$\frac{P_{FE}}{P_{AISC}}$
Mean	0.998	1.022
COV	0.067	0.127

Table 5: Effect of load eccentricity (e/D) ratio

Group	Column Designation	Column Properties				Axial Capacity		Comparison
		e/D	D/t	f'_c (MPa)	f_y (MPa)	P_{FE} (kN)	P_{AISC} (kN)	$\frac{P_{FE}}{P_{AISC}}$
1	C2D1E1F2	0.00	33.33	40	350	19279	18250	1.07
	C2D1E2F2	0.15	33.33	40	350	14086	13750	1.01
	C2D1E3F2	0.30	33.33	40	350	10934	10890	1.04
2	C2D2E1F2	0.00	41.67	40	350	17575	16400	1.09
	C2D2E2F2	0.15	41.67	40	350	12603	12310	1.01
	C2D2E3F2	0.30	41.67	40	350	9624	9931	1.06
3	C2D3E1F2	0.00	50.00	40	350	16235	15150	1.09
	C2D3E2F2	0.15	50.00	40	350	11563	11350	1.03
	C2D3E3F2	0.30	50.00	40	350	8744	9036	1.16

4.1 The effect of load eccentricity ratio (e/D)

The behaviour of CFST columns under bending induced by eccentrically applied axial load was found to be significantly affected by the initial load eccentricity ratio. This finding was obtained by dividing the initial eccentricity, e, of the applied axial load by the depth of the column cross-section, D. It served to reduce the load carrying capacity of the column as compared to a concentrically loaded column. Three groups of CFST columns were simulated to observe the effect of eccentricity, the groups having been formulated based on the D/t ratios. The load eccentricity ratios used for each group in this study were 0, 0.15, and 0.30, respectively. The effect of the load eccentricity ratio on the axial load capacity of the CFST columns was found to be significant, as shown in Table 5. The load carrying capacities of columns C2D1E2F2 and C2D1E3F2 were found to decrease by 27% and 43%, respectively, compared to C2D1E1F2 in Group 1. Similar percentages of variations were also observed in Groups 2 and 3.

The numerical capacities of these columns were compared with the AISC code-predicted capacity for these three e/D ratios, with the numerical capacities found to be higher than the code-predicted capacities (by about 6% on average). The ultimate load carrying capacities of these columns, it should be noted, are influenced by depth-to-thickness ratio (D/t). The percentage of load decrement due to eccentricity was found to be higher in Group 3 than in Group1. This was due to the lower steel tube thickness (t) of the columns in Group 3 compared to Group 1.

4.2 Effect of column depth to thickness (D/t)

The six columns the results of which are presented in Table 6, divided into two groups (Groups 4 and 5), were simulated numerically to observe the effects of column depth-to-thickness (D/t) on the compressive strength of the CFTS column. The columns in Group 4 (C2D1E1F2, C2D2E1F2 and C2D3E1F2) and Group 5 (C2D1E2F2, C2D2E2F2 and C2D3E2F2) had the same concrete compressive strength and steel strength with 40 MPa and 350 MPa, respectively. The depth-to-thickness (D/t) ratios of these columns were 33.33, 41.67 and 50 mm, respectively. The load carrying capacity of the CFST columns was found to increase with a decrease in D/t ratio. In Group 4, for example, reductions in D/t ratio from 50 to 41.67 and 33.33 were found to result in increases in load carrying capacity by 8% and 19%, respectively. Similarly, in Group 5, reduction of D/t ratio from 50 to 41.67 and 33.33 were found to increase the load carrying capacity by 9% and 22%, respectively, as shown in Table 6. The numerical load carrying capacities of these columns were then compared with the AISC (2010) code-predicted capacity. The code-predicted capacities were observed to be conservative as compared to the numerical results.

Table 6: Effect of column depth to thickness (D/t)

Groups	Column Designation	Column Properties				Axial Capacity		Comparison
		e/D	D/t	f'_c (MPa)	f_y (MPa)	P_{FE} (kN)	P_{AISC} (kN)	$\frac{P_{FE}}{P_{AISC}}$
4	C2D1E1F2	0.00	33.33	40	350	19279	18250	1.07
	C2D2E1F2	0.00	41.67	40	350	17575	16400	1.09
	C2D3E1F2	0.00	50.00	40	350	16235	15150	1.09
5	C2D1E2F2	0.15	33.33	40	350	14086	13750	1.00
	C2D2E2F2	0.15	41.67	40	350	12603	12310	0.99
	C2D3E2F2	0.15	50.00	40	350	11563	11350	0.93

6.1 Effect of concrete compressive strength (f'_c)

The compressive strength of concrete plays an important role in increasing the load carrying capacity of CFST column, thereby reducing the required column size. In this study, nine columns were simulated to observe the effect of concrete strength using varying the strengths of concrete (30 MPa, 40 MPa, and 50 MPa). These columns were divided into three groups (Groups 6 to 8), and all were simulated for constant eccentricity ratio and yield strength of steel with varying D/t ratios as shown in Table 7. The ultimate axial load of the column in Group 6, C2D1E2F2 (f'_c= 40 MPa) was increased by 11% compared to column C1D1E2F2 (f'_c= 30 MPa).

Table 7: Effect of concrete compressive strength (f'_c)

Group	Column Designation	Column Properties				Axial Capacity		Comparison
		e/D	D/t	f'_c (MPa)	f_y (MPa)	P_{FE} (kN)	P_{AISC} (kN)	$\frac{P_{FE}}{P_{AISC}}$
6	C1D1E2F2	0.15	33.33	30	350	12684	12230	0.98
	C2D1E2F2	0.15	33.33	40	350	14086	13750	1.00
	C3D1E2F2	0.15	33.33	50	350	15463	15080	1.02
7	C1D2E2F2	0.15	41.67	30	350	11150	10780	1.01
	C2D2E2F2	0.15	41.67	40	350	12603	12310	0.99
	C3D2E2F2	0.15	41.67	50	350	14050	13760	1.00
8	C1D3E2F2	0.15	50.00	30	350	10052	9861	1.01
	C2D2E2F2	0.15	50.00	40	350	11563	11460	0.93
	C3D2E2F2	0.15	50.00	50	350	13003	12910	0.96

Similarly, the axial capacity of column C3D1E2F2 (f'_c= 50 MPa) was increased by 10% compared to column C2D1E2F2 (f'_c= 40 MPa). The same load increment percentages were observed for the columns in Groups 7 and 8, while the load increment percentages were found to be comparatively lower when the concrete

strength increased from 40 MPa to 50 MPa, this due to the brittle behaviour of concrete. Similar behavior can be observed among these columns when their ultimate capacities are calculated using the equations given by AISC (2010).

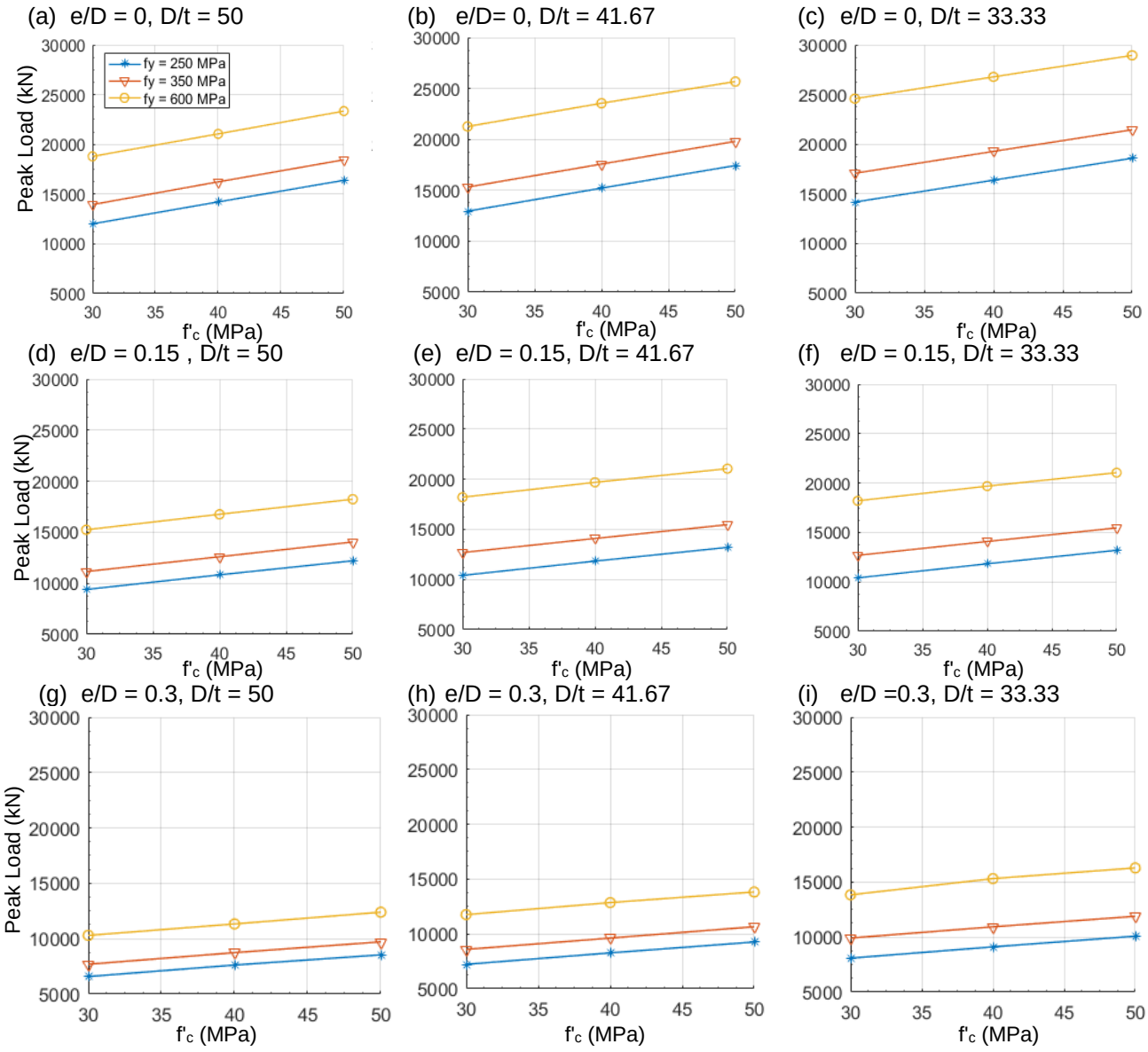

Figure 5: Effects of steel yield stress and concrete strength for different D/t ratio on the ultimate strength of CFST columns

4.4 Effect of steel yield strength (f_y)

Twelve columns divided into four groups (Groups 9 to 12) were simulated numerically to observe the effects of steel yield strength (f_y) on the ultimate axial load capacity of the CFST column. Three different steel strengths (250, 350 and 600 MPa) were considered in this study. These columns were simulated for concentric and eccentric (e/D= 0.15) axial load with two concrete strengths (30 MPa and 50 MPa). The details of the geometric and materials properties of these columns are shown in Table 8. The load carrying capacity of column C1D3E1F2 was found to be 16% higher than that of column C1D3E1F1 in Group 9,

where the steel strength varied from 250 to 350 MPa. Similarly, column C1D3E1F3 was found to be 35% higher than column C1D3E1F2, where the steel strength varied from 350 to 600 MPa. All the columns in Group 9 were simulated with a concrete strength of 30 MPa. Among the columns in Group 10 constructed with 50 MPa, load carrying capacity increased by 11% in column C3D3E1F2 (f_y = 350 MPa) compared to column C3D3E1F1 (f_y = 250 MPa). Again, the load carrying capacity of column C3D3E1F3 (f_y = 600 MPa) increased by 26% compared to column C3D3E1F2 (f_y = 350 MPa). It occurred due to the brittle behaviour of higher strength concrete (50 MPa) compared to lower strength concrete (30 MPa). Similarly, percentages of load carrying capacity also increased in the columns in Groups 11 and 12 when steel strength increased from 250 to 350 and 350 to 600 MPa.

Table 8: Effect of steel yield strength (f_y)

Group	Column Designation	Column Properties				Axial capacity		comparison
		e/D	D/t	f'_c (MPa)	f_y (MPa)	P_{FE} (kN)	P_{AISC} (kN)	$\frac{P_{FE}}{P_{AISC}}$
9	C1D3E1F1	0.00	50.00	30	250	12012	11110	1.10
	C1D3E1F2	0.00	50.00	30	350	13949	13130	1.08
	C1D3E1F3	0.00	50.00	30	600	18792	17910	1.05
10	C3D3E1F1	0.00	50.00	50	250	16388	15150	1.11
	C3D3E1F2	0.00	50.00	50	350	18449	17170	1.10
	C3D3E1F3	0.00	50.00	50	600	23346	21770	1.07
11	C1D3E2F1	0.15	50.00	30	250	8619	8419	1.04
	C1D3E2F2	0.15	50.00	30	350	10052	9861	1.01
	C1D3E2F3	0.15	50.00	30	600	13003	13300	0.96
12	C3D3E2F1	0.15	50.00	50	250	11414	11410	0.98
	C3D3E2F2	0.15	50.00	50	350	13003	12910	0.95
	C3D3E2F3	0.15	50.00	50	600	16445	16190	1.09

5 Conclusions

This paper presents an extensive numerical study investigating the behaviour of square CFST columns under concentric and eccentric loading conditions. Available experimental results were used to further verify the numerical modelling technique. Then, the validated FE modelling technique was used to perform a comprehensive parametric study varying the load eccentricity ratio (e/D), overall column depth-to-thickness ratio (D/t), concrete compressive strength (f'_c), and yield strength (f_y) of steel.

The major findings from the current study are summarized below:

1. The FE models were found to be capable of predicting the test capacity of CFST columns with good accuracy with a mean value of 0.998 and COV of 0.067.
2. The ultimate axial capacity of CFST columns increased with the increase in concrete compressive strength and yield strength of steel. However, the increase in capacity was more pronounced in case of yield strength of steel compared to compressive strength of concrete. This is mainly due to the brittle failure of 50 MPa concrete compared to 30 MPa concrete.
3. The higher load eccentricity ratio (e/D) significantly reduced the capacity of CFST columns. This may be attributable to the increase in moment corresponding to ultimate load along with a second-order effect.
4. The load carrying capacity of CFST columns increased with the decrease in column depth-to-thickness (D/t) ratio (average increase was 22%).
5. The AISC code-predicted capacity was found to be conservative compared with the experimental and FE results. The mean value of the ratios of the FE results and AISC predictions was found to be 1.03 with a COV of 0.08. This is mainly due to the strength reduction factor of 0.85 used in the AISC code.

References

ABAQUS Version 6.14, *user documentation* [online]. Providence, RI: DassaultSystemes.

Tao, Z., Wang, Z. and Yu, Q. (2013). Finite element modelling of concrete-filled steel stub columns under axial compression. *Journal of Constructional Steel Research*, 89, pp.121-131.

Schneider, S. (1998). Axially Loaded Concrete-Filled Steel Tubes. *Journal of Structural Engineering*, 124(10), pp.1125-1138.

Han, L., Yao, G. and Zhao, X. (2005). Tests and calculations for hollow structural steel (HSS) stub columns filled with self-consolidating concrete (SCC). *Journal of Constructional Steel Research*, 61(9), pp.1241-1269.

Han, L. (2002). Tests on stub columns of concrete-filled RHS sections. *Journal of Constructional Steel Research*, 58(3), pp.353-372.

Chen, C., Ko, J., Huang, G. and Chang, Y. (2012). Local buckling and concrete confinement of concrete-filled box columns under axial load. *Journal of Constructional Steel Research*, 78, pp.8-21.

Papanikolaou, V. and Kappos, A. (2007). Confinement-sensitive plasticity constitutive model for concrete in triaxial compression. *International Journal of Solids and Structures*, 44(21), pp.7021-7048.

Yu, T., Teng, J., Wong, Y. and Dong, S. (2010). Finite element modeling of confined concrete-I: Drucker–Prager type plasticity model. *Engineering Structures*, 32(3), pp.665-679.

Wang, B. (2011). Experimental Behavior of Concrete-Filled Square Steel Tube of Mid and Long Columns Subjected to Eccentric Compression. *Advanced Materials Research*, 255-260, pp.118-122.

Shieh, S.S., Chang, C.C. and Jong, J.H., 2003, October. Structural design of composite super-columns for the Taipei 101 Tower. In *Proceedings of International Workshop on Steel and Concrete Composite Constructions* (pp. 25-33).

Shams, M. and Saadeghvaziri, M.A., 1997. State of the art of concrete-filled steel tubular columns. *ACIStructural Journal*, *94*(5), pp.558-571.

Han, L.H., Yao, G.H. and Tao, Z., 2007. Performance of concrete-filled thin-walled steel tubes under pure torsion. *Thin-Walled Structures*, *45*(1), pp.24-36.

Sakino, K &Tomii, M & Watanabe, K. (1985). Sustaining load capacity of plain concrete stub columns by circular steel tubes. *Proceeding of the International Speciality Conference on Concrete-Filled Steel Tubular Structure*. 112-118. ASCCS, Harbin, China

Huang, F., Yu, X. and Chen, B., 2012. The structural performance of axially loaded CFST columns under various loading conditions. *Steel & Composite Structures*, *13*(5), pp.451-471.

Liu, J., Zhou, X. and Zhang, S., 2008. Seismic behaviour of square CFT beam–columns under biaxial bending moment. *Journal of Constructional Steel Research*, *64*(12), pp.1473-1482.

Zhang, G.W., Xiao, Y. and Kunnath, S., 2009. Low-cycle fatigue damage of circular concrete-filled-tube columns. *ACI Structural Journal*, *106*(2), p.151.

Perea, T., Leon, R.T., Hajjar, J.F. and Denavit, M.D., 2014. Full-scale tests of slender concrete-filled tubes: Interaction behavior. *Journal of Structural Engineering*, *140*(9), p.04014054.

Jiang, A.Y., Chen, J. and Jin, W.L., 2013. Experimental investigation and design of thin-walled concrete-filled steel tubes subject to bending. *Thin-Walled Structures*, *63*, pp.44-50.

Yang, Y.F. and Ma, G.L., 2013. Experimental behaviour of recycled aggregate concrete filled stainless steel tube stub columns and beams. *Thin-Walled Structures*, *66*, pp.62-75.

Liu, D. and Gho, W.M., 2005. Axial load behaviour of high-strength rectangular concrete-filled steel tubular stub columns. *Thin-Walled Structures*, *43*(8), pp.1131-1142.

Thai, H.T., Uy, B., Khan, M., Tao, Z. and Mashiri, F., 2014. Numerical modelling of concrete-filled steel box columns incorporating high strength materials. *Journal of Constructional Steel Research*, *102*, pp.256-265.

Khan, M., Uy, B., Tao, Z. and Mashiri, F., 2017. Concentrically loaded slender square hollow and composite columns incorporating high strength properties. *Engineering Structures*, *131*, pp.69-89.

Khan, M., Uy, B., Tao, Z. and Mashiri, F., 2017. Behaviour and design of short high-strength steel welded box and concrete-filled tube (CFT) sections. *Engineering Structures*, *147*, pp.458-472.

Ellobody, E., Young, B. and Lam, D., 2006. Behaviour of normal and high strength concrete-filled compact steel tube circular stub columns. *Journal of Constructional Steel Research*, *62*(7), pp.706-715.